Dependence of magnetization dynamics on magnetostriction in NiFe alloys

R. Bonin
Physics Department, Politecnico di Torino, I-10129 Torino, Italy and IEN Galileo Ferraris (INRIM), I-10135 Torino, Italy

M. L. Schneider[a] and T. J. Silva
National Institute of Standards and Technology, Boulder, Colorado 80305

J. P. Nibarger
Sun Microsystems, One StorageTek Drive, Louisville, Colorado 80028

(Received 5 April 2005; accepted 4 November 2005; published online 23 December 2005)

We present a quantitative, systematic study of the effect of magnetostriction on the dynamical properties in NiFe alloys. Both the ferromagnetic resonance frequency and the damping times are correlated to the magnetostriction. In addition, we find that the Gilbert damping parameter varies by more than 100% over the range of Ni percentage tested (61.9%–86.7%). © *2005 American Institute of Physics*. [DOI: 10.1063/1.2143121]

I. INTRODUCTION

The nominally zero magnetostriction of $Ni_{80}Fe_{20}$ has long been seen as a desirable property by the magnetic recording industry. However, the details of the magnetostriction effect on the dynamics in NiFe films are not well understood. For this reason we have studied the magnetodynamics in $Ni_{(1-X)}Fe_X$ thin films, in which the magnetostriction coefficient is adjusted by varying the Ni-to-Fe ratio. This was done in order to determine whether there is a relationship between the magnetodynamical and magnetoelastic properties in this material system.

Measurements were performed on a series of thin NiFe films grown around the nominally zero magnetostriction Permalloy composition of $Ni_{80}Fe_{20}$ (subscripts denote atomic percentage). By changing the Ni-to-Fe ratio we were able to vary the magnetostriction constant λ_s from -0.7×10^{-5} to 1.5×10^{-5}. We found a systematic impact on the dynamical response of the thin films. Both the ferromagnetic resonance frequency and the decay rate are affected. The films are most heavily damped when the magnetostriction is at the negative extreme and are least damped at the positive extreme. In addition, previous work has found a rotatable anisotropy component in dynamic measurements that may also be related to the magnetostriction.[1,2] We have confirmed that the magnetostriction does influence the rotatable anisotropy. Furthermore, we found that there is a local minimum in the rotatable anisotropy for the samples with magnetostriction constants near zero.

II. SAMPLE PREPARATION

The samples used were 50 nm polycrystalline thin films with varying ratios of Ni and Fe covering a range from $Ni_{61.9}Fe_{38.1}$ to $Ni_{86.7}Fe_{13.3}$. The films were cosputtered from Ni and Fe targets onto 38 mm×5 mm×380 μm Si (100) substrates. A 5 nm Ta seed layer was used to promote adhesion of the films. A 5 nm Ta capping layer was used to protect the films against oxidation. The films were grown by dc magnetron sputtering in a chamber with a base pressure of 10^{-6} Pa. In order to improve homogeneity a rf bias was applied to the samples during growth. All films were grown in a 32 kA/m (400 Oe) field to induce a uniaxial anisotropy.

III. STATIC MEASUREMENTS

The quasistatic magnetic properties of the samples were characterized using a low-frequency (50 Hz) inductive magnetometer. In order to determine the uniaxial anisotropy field $H_k^{(2)}$, we measured the hard-axis hysteresis loops as function of an applied easy-axis bias field H_b^{EA}. This process was previously described in detail[3] and was used to obtain $H_k^{(2)}$ for all samples; see Table I for the values of $H_k^{(2)}$ for all of the samples.

The samples were measured with x-ray fluorescence (XRF) in order to more precisely determine the Ni-to-Fe ratio. The magnetostriction coefficients λ_s were obtained by optically measuring the mechanical deflection of a sample in response to an applied magnetic field.[4] Figure 1 shows λ_s

TABLE I. Magnetic and magnetostrictive characteristics of the samples.

Stoichiometry (% Ni)	λ_s	M_S (kA/m)	$H_k^{(2)}$ (A/m)	Error $H_k^{(2)}$ (A/m)
86.7	-6.58×10^{-6}	754.01	492.72	4.64
84.4	-5.51×10^{-6}	782.27	440.32	20.00
83.9	-2.71×10^{-6}	788.41	447.68	3.84
80.9	-9.72×10^{-7}	825.26	505.84	12.08
79.4	6.65×10^{-8}	843.69	479.20	2.64
79.3	7.59×10^{-7}	844.92	480.56	8.32
76.6	3.12×10^{-6}	878.09	413.52	17.6
76.3	4.10×10^{-6}	881.77	439.60	19.12
75.1	7.28×10^{-6}	896.52	510.08	18.4
73.0	6.97×10^{-6}	922.31	410.32	11.92
72.4	7.53×10^{-6}	929.68	570.32	9.12
70.9	8.57×10^{-6}	948.11	454.08	13.36
70.7	1.08×10^{-5}	950.57	720.48	6.72
61.9	1.47×10^{-5}	1058.7	683.84	8.40

[a]Electronic mail: michael.schneider@boulder.nist.gav

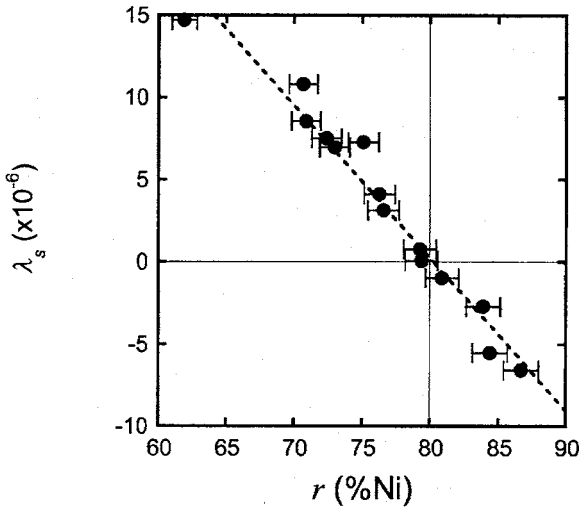

FIG. 1. The value of the magnetostriction coefficients for all samples plotted vs the percentage of Ni. The uncertainty in the magnetostriction coefficient is smaller than the size of the data points. The slope, in percent, and the intercept of a linear regression fit to the data, shown as a dotted line, are $(-9.3\pm0.5)\times10^{-7}$ and $(7.5\pm0.4)\times10^{-5}$, respectively.

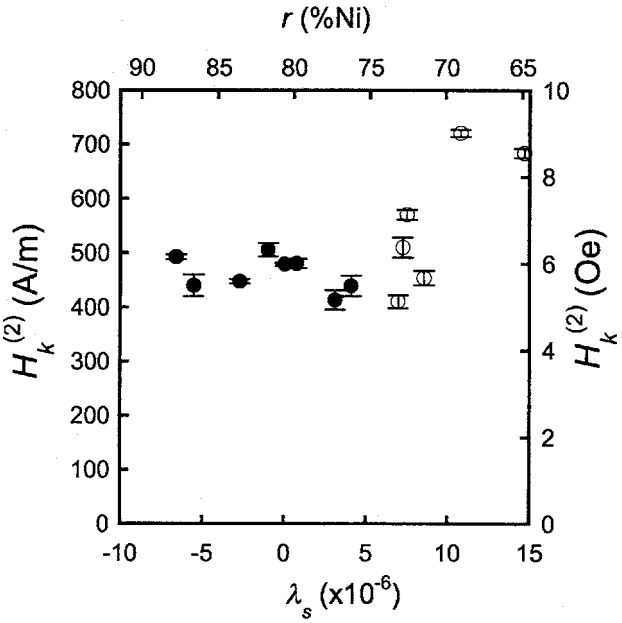

FIG. 2. The dependence of the uniaxial anisotropy $H_k^{(2)}$ on magnetostriction coefficient λ_S. The data with Fe$\geqslant$25% are shown with open circles. The top axis uses a linear extrapolation from the fit in Fig. 1 to provide the approximate Ni percentage.

versus stoichiometry for our samples. The error bars on λ_s are smaller than the data points and were determined from multiple measurements and multiple mountings of the samples. The dependence is linear when the Ni fraction is near 80%. The calibration of the growth parameters was checked with XRF for half of the samples. The XRF measurements were consistent for all samples and were used to set the error bars displayed in Fig. 1. Fitting our data to a line, we find that the zero magnetostriction crossing occurs at Ni=79.9±0.8%. This agrees, within error, with the accepted value for the zero crossing of Ni=80%.[5–7] The measured values of λ_s for each sample can be found in Table I.

Figure 2 shows the quasistatic anisotropy $H_k^{(2)}$ as a function of the measured magnetostriction. There is no clear dependence of $H_k^{(2)}$ on the magnetostriction coefficient. However, for the samples that have the most Fe, the anisotropy is larger, while for the rest of the sample $H_k^{(2)}$ is independent of stoichiometry. The disturbance in the uniaxial anisotropy for higher Fe content might be attributed to structural changes in the alloy itself; there is a miscibility gap between the α-Fe phase and the ordered $FeNi_3$ phase starting at Fe=25% at room temperature according to the phase diagram of NiFe alloys.[8] This suggests that the formation of α-Fe precipitates within the Permalloy matrix is thermodynamically favored with the addition of more Fe for Fe$>$25%. If we exclude the samples with Fe=25% or more, then $H_k^{(2)}$ simply fluctuates about a mean value of 460±30 A/m.

IV. DYNAMIC MEASUREMENTS

The dynamic measurements were performed with a pulsed inductive microwave magnetometer[9] (PIMM) with a coplanar waveguide (CPW) containing a 220-μm-wide center conductor of 50 Ω characteristic impedance. A commercial pulse generator provided pulses with 50 ps rise time, 10 ns duration, and 100 kHz repetition rate. Using the Karlquist equation[10] for the field produced by a current strip, we calculated that our 5 V pulses produced a field pulse of 166 A/m (2 Oe) at the film surface. The samples were placed on the CPW with a single layer of Kapton tape of 50 μm thickness, used as an insulating spacer between the thin-film surface and the CPW. Orthogonal Helmholtz coil pairs were used to produce the static bias and saturation fields used in the measurements; the two fields were parallel and perpendicular to the direction of the CPW center conductor, respectively, and both are in the plane of the film. The field was calibrated to better than 1% variation across the area of the sample. The precessional response was measured with a 20 GHz digital sampling oscilloscope. The precessional frequency ranged from 0.85 to 4.29 GHz and was well within the measurable bandwidth of the system.[11]

To obtain the time domain signal, we performed a two-step measurement. First, a longitudinal bias field H_b was applied along the easy axis of the sample while the voltage wave-form for the transmitted pulse was measured. Next, a transverse saturation field was applied along the hard axis of the film in the direction of the pulse field during a second wave-form acquisition. The two data sets were subtracted from one another to obtain the dynamic response of the sample to the field pulse. The precessional response of the samples was converted from the time domain into the frequency domain via a fast Fourier transform (FFT). The precessional frequency was determined by measuring the zero crossing of the real part of the susceptibility.[12] In addition, the decay rate at each field was determined by fitting the imaginary peak to the standard response function.[12]

The FFT of our data can be related to the susceptibility spectrum $\chi(\omega)$ found by linearizing the Landau-Lifshitz-Gilbert (LLG) equation for a small excitation field; with a bias field along the easy axis we obtained[13]

$$\chi(\omega) = \frac{\omega_m(\omega_m + i\alpha\omega)}{-\omega^2 + (\omega_k + \omega_b)\omega_m + i\omega\alpha\omega_m}, \quad (1)$$

where $\omega_m = \gamma\mu_0 M_s$, $\omega_b = \gamma\mu_0 H_b$, $\omega_k = \gamma\mu_0 H_k^{\mathrm{dyn}}$, $\gamma = g\mu_b/\hbar$, μ_0 is the permeability of free space, α is the Gilbert damping parameter, M_s is the saturation magnetization, and H_k^{dyn} is the total effective dynamic anisotropy field.

The values for H_k^{dyn} as measured by the PIMM must be corrected for internal dipolar field contributions caused by the finite width of the CPW center conductor. The finite CPW center conductor width acts as a source of additional stiffness field $H_k^{\mathrm{MSSW}} = (\pi/4)M_s(\delta/w)$, where w is the center conductor width and δ is the sample thickness.[14] In the limit of $M_s \gg H_b + H_k^{\mathrm{dyn}}$ and $\alpha \ll 1$, Eq. (1) is well approximated by

$$\chi(\omega) \approx \left(\frac{\omega_M}{\omega_b + \omega_k}\right)\frac{\omega_0^2}{\omega_0^2 - \omega^2 + i\omega\alpha\omega_m}, \quad (2)$$

where $\omega_0^2 = \omega_m(\omega_k + \omega_b)$ is the Kittel equation for the resonance frequency ω_0^2.

To determine H_k^{dyn} the samples were measured with the easy axis aligned along the CPW center conductor. Accurate determination of the effective total anisotropy relies upon the proper orientation of the sample's easy axis along the applied longitudinal bias field H_b. To improve the accuracy of the alignment of the easy axis, the resonance frequency was obtained as a function of varying angle θ between the easy axis of the film and the CPW center conductor, ranging from $-180°$ to $180°$ in $14.85°$ increments. These measurements were taken with an applied bias field along the CPW center conductor of 8 kA/m (100 Oe). The resonance frequency $f_0 = \omega_0/2\pi$ was extracted from the data at every angle θ. From the Kittel equation we expect that f_0^2 vs θ should exhibit a $\cos(2\theta)$ dependence due to the uniaxial component of anisotropy in the samples.[2] Using this approach, we were able to determine the easy-axis angle with an uncertainty of $0.4°$.

With the easy axis aligned parallel to the CPW center conductor, we performed measurements in which we varied H_b using 80 A/m (1 Oe) steps from 0 A/m (0 Oe) to 12 800 A/m (160 Oe). For every value of H_b, we determined f_0 as derived from the FFT of the time-domain data. We determined H_k^{dyn} by plotting f_0^2 versus the applied bias field H_b, then applied linear regression to the data in accordance with the low-field approximation ($M_s \gg H_b + H_k$) to the Kittel equation:

$$\omega_0^2 \approx (\gamma\mu_0)^2 M_s(H_b + H_k^{\mathrm{dyn}}), \quad (3)$$

where H_k^{dyn} is the anisotropy field obtained using the dynamical measurements with the PIMM.[2] In addition to extracting H_k^{dyn}, determination of the slope of the line gives the value of the Landé g factor using Eq. (3). Note that this extraction of g presumes prior knowledge of the saturation magnetization M_s. We used the previously determined value for M_s of a 50 nm $Ni_{80}Fe_{20}$ film of 831.9 kA/m.[15] However, M_s will depend on the Ni:Fe ratio. Near the $Ni_{80}Fe_{20}$ stoichiometry we approximated the magnetization variation as $M_S(r) = M_{\mathrm{NiFe}} + (r - 0.8)(M_{\mathrm{Ni}} - M_{\mathrm{Fe}})$, where $M_{\mathrm{NiFe}} = 831.9$ kA/m (10 450 Oe), $M_{\mathrm{Ni}} = 485$ kA/m (6095 Oe), and $M_{\mathrm{Fe}} = 1707$ kA/m (21 451 Oe) are the saturation magnetizations of $Ni_{80}Fe_{20}$, Ni, and Fe, respectively, and r is the fraction of Ni for a given sample. Values of M_s were estimated in this manner for each sample and used in the calculation of g. We find that $g = 2.06 \pm 0.03$, and there is no clear dependence of the g factor on magnetostriction or stoichiometry.

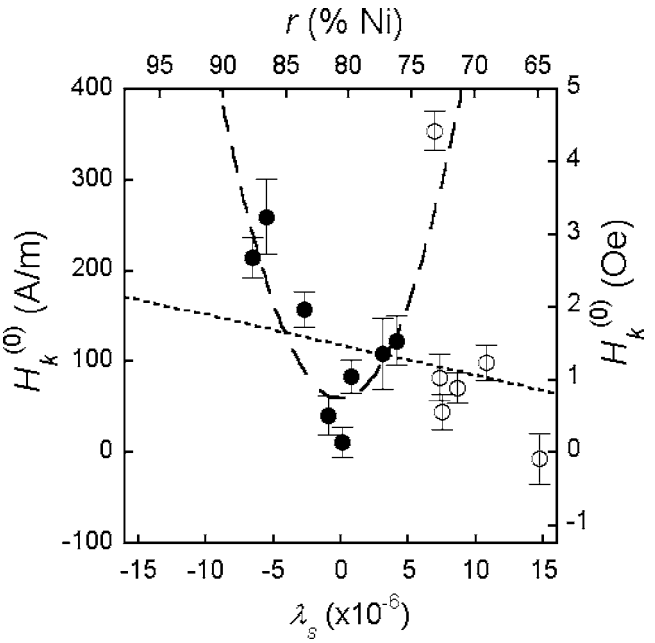

FIG. 3. The rotatable anisotropy $H_k^{(0)}$ vs magnetostriction λ_S is shown. The open circles correspond to the data with Fe $\geq$ 25%. The linear fit (shown as a dotted line) is over all of the data, while the parabolic fit is only on the samples with Fe $<$ 25%. One would expect a quadratic dependence (shown as a dashed line) of the amplitude of $H_k^{(0)}$ if it is the result of plastic deformations in the lattice induced by the magnetostriction. The top axis uses a linear extrapolation from the fit in Fig. 1 to provide the approximate Ni percentage.

We determined H_k^{dyn} from the plot of f_0^2 vs H_b, where, as can be seen from Eq. (3), the extrapolated field intercept H_b' at $\omega_0 = 0$ is related to the dynamic anisotropy through $H_k^{\mathrm{dyn}} = -H_b'$. Once we obtained H_k^{dyn}, we subtracted $H_k^{(2)}$ (as determined from the quasistatic measurement[2]) and H_k^{MSSW} (the correction for dipole fields due to the finite CPW center conductor width[14]) to determine $H_k^{(0)}$. After subtraction of $H_k^{(2)}$ and H_k^{MSSW} from H_k^{dyn}, there remains a nonzero quantity due to the presence of a rotatable anisotropy $H_k^{(0)}$.[2]

Figure 3 shows $H_k^{(0)}$ as a function of the magnetostriction coefficient. Fitting all of the data to a linear fit we find a negative slope equal to $-3 \times 10^6 \pm 1 \times 10^6$ A/m per λ_s and an offset of 119 ± 7 A/m. However, the normalized χ^2 for this fit is 18. If we exclude the Fe-rich samples on the assumption that they may have α-Fe precipitates, as suggested by the static anisotropy data for Fe $\geq$ 25%, then there is a minimum near $\lambda_s = 0$. This suggests that for samples with $|\lambda_s| < 7 \times 10^{-6}$, the rotatable anisotropy may be a result of the nonzero magnetostriction present in NiFe alloys near the $Ni_{80}Fe_{20}$ composition. If one fits the data with Fe $<$ 25% to a

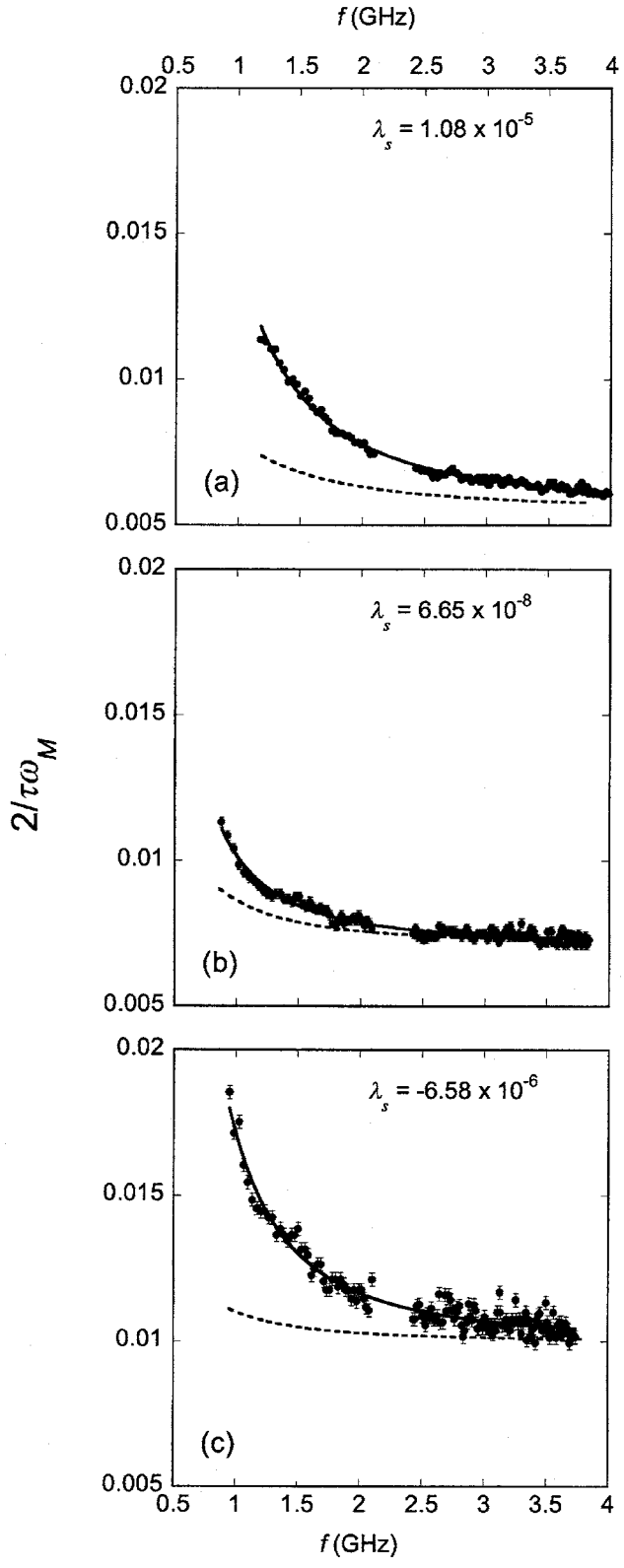

FIG. 4. The decay rate vs frequency for three samples of varying magnetostriction. The solid curves are fits to a power-law function. The dashed curves are predictions based upon the spin-wave theory of Counil *et al.* (see Ref. 24). Figure 4(a) is for a sample with positive magnetostriction coefficient, 4(b) is for a sample with negligible magnetostriction coefficient, and 4(c) is for a sample with a negative magnetostriction coefficient.

parabola, the normalized $\chi^2=3$. While this is a substantial improvement over the linear fit, it is not sufficient to exclude the null hypothesis that $H_k^{(0)}$ and λ_s are not correlated.

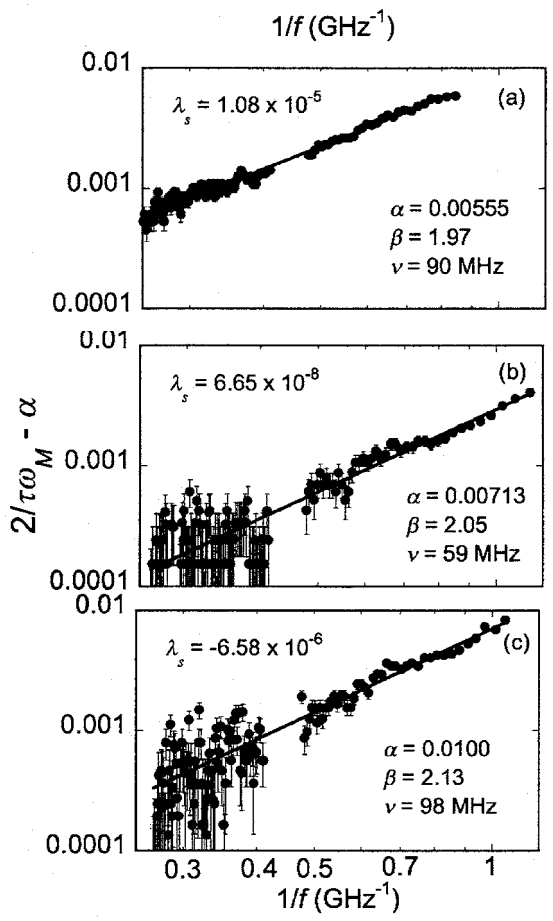

FIG. 5. Log-log plots of normalized free-induction decay rate as a function of precession frequency. The line is a power-law fit observed over a frequency range that spans an order of magnitude. Figure 5(a) is for a sample with positive magnetostriction coefficient, 5(b) is a sample with negligible magnetostriction coefficient, and 5(c) is a sample with a negative magnetostriction coefficient.

V. DECAY RATE ANALYSIS

Figures 4(a)–4(c) show how the magnetization decay rate varies as a function of resonance frequency for three samples with positive, negligible, and negative magnetostriction coefficients, respectively. The relaxation time τ is the exponential time constant associated with the free induction decay of the gyromagnetic precession, and τ has been normalized with respect to the saturation magnetization in order to allow for comparison with the Gilbert damping parameter.

As has been previously observed, there is a significant dependence of the decay rate upon the resonance frequency.[16] We have fitted the data to a power law of the form

$$\frac{2}{\tau\omega_M} = \alpha + \left(\frac{\nu}{f}\right)^{\beta}, \tag{4}$$

where α is the LLG damping parameter and ν is the frequency-scaling parameter for the power-law fits. From such fits, we determined that the power-law exponent $\beta = 2.2 \pm 0.07$ for all of the samples measured and shows no clear trend with λ_s. The normalized χ^2 values for all the fits are approximately unity, suggesting that a power law is an appropriate model for the resonance frequency dependence

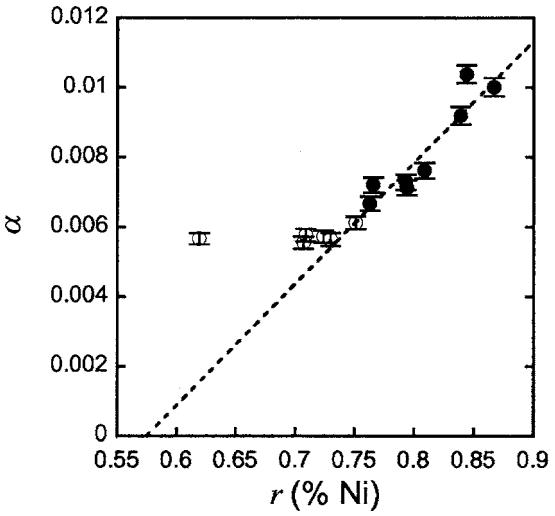

FIG. 6. The LLG damping parameter is plotted as a function of r (Ni percentage) in the sample alloy. Linear regression (shown as a dotted line) was applied to the data with Fe$<$25%, resulting in a regression coefficient of 0.93.

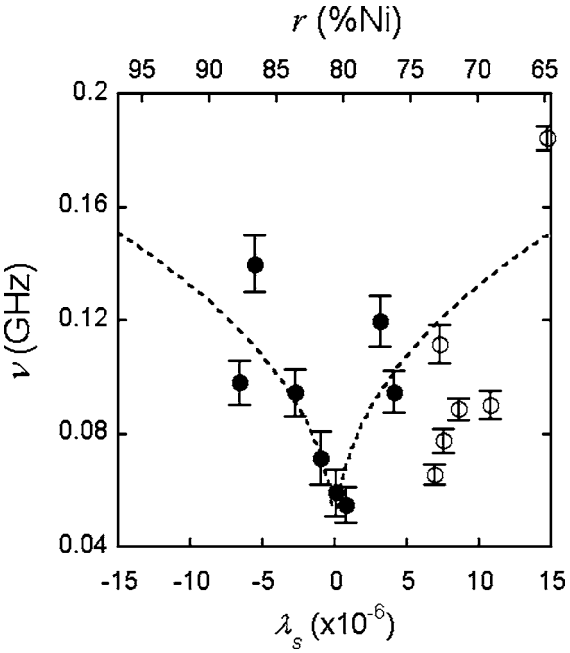

FIG. 7. The power-law scaling frequency ν is plotted vs the magnetostriction coefficient λ_S. The dotted curves represent a $\beta=2.2$ scaling from Eq. (A10) fit to the data with Fe$<$25%. The open circles correspond to the data with Fe$>$25%. The top axis uses a linear extrapolation from the fit in Fig. 1 to provide the approximate Ni percentage.

of free induction decay. A conventional model based on inhomogeneous line broadening would predict $\beta=1$.[17] Therefore, the increase in the decay rate at low frequencies is not simply the result of a nonuniform internal field. Figures 5(a)–5(c) show log-log plots of the same decay rate data shown in Figs. 4(a)–4(c), clearly demonstrating the supralinear power-law dependence of the damping upon the inverse precession frequency.

Fitting the data in Figs. 4(a)–4(c) with a power-law function yields values of $\alpha=0.0056$, 0.0071, and 0.0100, respectively. In all three cases, the data at the highest frequencies are within 10% of the fitted values for the LLG damping parameter. This suggests that the range of measured frequencies is sufficient to accurately determine α.

In Fig. 6, we present the dependence of α on Ni percentage. Note that the LLG damping is neither maximized nor minimized at the magnetostriction zero point of 80% Ni. This suggests that the high-frequency damping is actually a direct function of the stoichiometry of the sample, with Ni-rich Permalloy exhibiting a larger damping than Fe-rich Permalloy. However, the damping is independent of Ni concentration for Ni$<$75%. Again, the formation of an inhomogeneous phase mixture for Fe$>$25% may explain this observation. Excluding the Fe-rich samples, the damping varies linearly with the Ni content. The data with Fe$<$25% were fitted to

$$\alpha = A + Br, \tag{5}$$

where r is the relative Ni concentration. The fitted parameters are $A=-0.02\pm0.002$ and $B=0.035\pm0.002$. Thus, changing the Ni content in Permalloy by as little as 20% can change the LLG damping by as much as 100%. We speculate that this is the result of the itinerant nature of ferromagnetism in Ni,[18] which could result in enhanced magnon-electron scattering rates, but only in the case of a pure metallic phase.

In Fig. 7 we examine the power-law scaling frequency ν as a function of λ_s. We find that there is no clear trend in the power-law scaling as a function of λ_s. However, if we exclude the samples with Fe$\geqslant$25%, then there is a minimum in ν when the magnetostriction coefficient is near zero, this would suggest that the low-energy spin decay rate is enhanced by an increase in $|\lambda_s|$.

To see if there is a common physical mechanism underlying both rotatable anisotropy and an enhanced decay rate at low frequencies, we can examine the correlation between $H_k^{(0)}$ and ν. In Fig. 8 we plot $H_k^{(0)}$ vs ν; using the student T test, we find that there is a highly significant correlation between these two extracted parameters, with a correlation coefficient of $R=0.79$, though only if we exclude the samples with Fe$\geqslant$25%. If we examine the correlation between $H_k^{(0)}$ vs ν for all samples, we find that $R=0.08$. From a best fit to the limited data set, we find that $\nu \cong \kappa(2\pi/\gamma\mu_0)H_k^{(0)}+\nu_0$ with $\kappa\approx7.9$ and $\nu_0\approx0.06$ GHz.

VI. DISCUSSION

Both anisotropy and magnetostriction are attributed to spin-orbit coupling, insofar as both effects require a connection between spin orientation and crystal lattice. However, it is generally assumed that an isotropic strain of the crystal lattice, as is expected for a sputter-deposited thin film, would not affect the in-plane anisotropy. As seen for the samples with Fe$<$25% in Fig. 2 we find that the uniaxial component of the anisotropy $H_k^{(2)}$ does not appear to be affected by magnetostriction. Instead, there seems to be a correlation between rotatable anisotropy $H_k^{(0)}$ and magnetostriction. This suggests that the rotatable anisotropy could be explained in terms of magnetoelastic tensor components, which relate deformation of the crystal lattice to magnetic energy terms. The fact that the anisotropy has a rotatable nature (i.e., the axis of

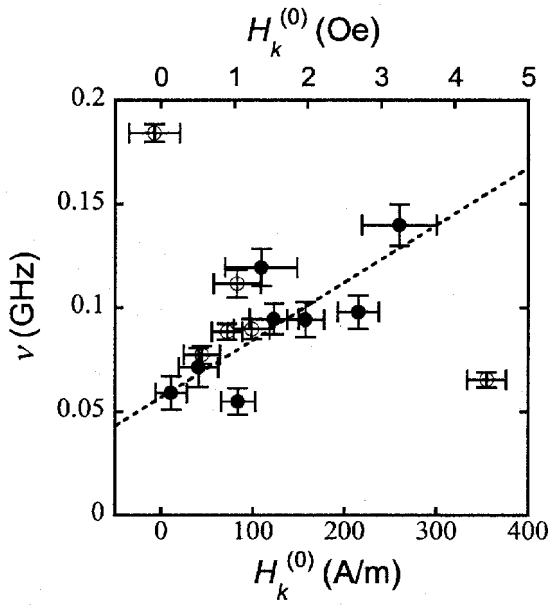

FIG. 8. The correlation plot of ν vs $H_k^{(0)}$ for data with Fe$<25\%$ was fitted by linear regression (shown as a dotted line) yielding a correlation coefficient of $R=0.79$. This value of R corresponds to a highly significant correlation with less than 0.1% chance that the data are randomly correlated.

broken symmetry is established by the alignment of the magnetization in a given direction for an extended duration of time) would imply that the coupling is the result of the plastic deformation of the crystal lattice which cannot follow the rapid variations in the magnetization direction during a pulsed excitation. Initial calculations suggest that this is a viable explanation for the observed phenomena.[19]

We can estimate the energy associated with such self-induced plastic strain in a straightforward manner. The effective anisotropy due to strain in a magnetic material is given by[20]

$$H_k^{\text{eff}} = B_1 e_{xx} \prod \left(\frac{1+\upsilon}{\mu_0 M_s} \right), \tag{6}$$

where e_{xx} is the total strain, B_1 is the magnetoelastic coupling coefficient, and υ is Poisson's ratio. For a magnetically saturated and unrestricted isotropic bulk sample, both B_1 and e_{xx} are proportional to the magnetostriction, with $e_{xx}=-\lambda_s$ and $B_1=-3/2(\lambda_s E)/(1+\upsilon)$, where E is Young's modulus relating mechanical stress and strain in the given material.[20] Thus, for a bulk sample, the effective self-induced anisotropy depends quadratically on magnetostriction, with

$$H_k^{\text{eff}} = \lambda_s^2 \frac{3E}{2\mu_0 M_s}. \tag{7}$$

We propose that the rotatable anisotropy can also be expressed in terms of a quadratic dependence on magnetostriction, but the bulk value for Young's modulus is replaced by an effective coefficient $G \doteq \sigma_m / e'_{xx}$ that relates magnetostrictive stress to the plastic component of strain in our specific thin-film geometry, where σ_m is the magnetostrictive stress and e'_{xx} is the plastic component of strain. Thus, our expression for the rotatable anisotropy is

$$H_k^{(0)} = \lambda_s^2 \frac{3G}{2\mu_0 M_s}. \tag{8}$$

Fitting of the data with Fe$<25\%$ in Fig. 3 to Eq. (8) yields $G=4200$ GPa. In contrast, $E \approx 200$ GPa for most metals.[20] Hence, the plastic component of strain associated with the rotatable anisotropy appears to be 21 times less susceptible to magnetostrictive-induced stress than the elastic strain components.

The supralinear dependence of the decay rate upon the period of spin precession is not yet understood. However, we find that the phenomenological correlation of the relaxation enhancement with the rotatable anisotropy suggests that the fundamental mechanism behind both effects is tied to the *plastic* deformation of the crystal lattice via spin-orbit coupling. This is to be distinguished from magnon-phonon scattering processes that depend upon the energy associated with *elastic* crystal deformations.

While a rotatable anisotropy might be attributed to the average plastic strain induced due to magnetostriction, the effect of strain on damping is most likely a result of fluctuations about the mean. Such local fluctuations in the strain would be consistent with a microscopic picture whereby the system hops between metastable atomic arrangements. (A description based on transitions between local minima in the energy surface is mandated by any system with some degree of mechanical hysteresis, i.e., plastic strain.) In turn, the hopping of the crystal structure between metastable states would cause fluctuations in the local field due to spin-orbit interactions (i.e., magnetostriction), resulting in dephasing of the spin precession.

A description of fluctuation processes that affect damping during the magnetization reorientation process requires nonequilibrium statistical mechanics. The observation of a power-law scaling for the decay rate at low frequencies suggests an analysis based on self-organized criticality (SOC).[21,22] In the SOC picture, systems that are driven far from equilibrium tend to become critical due to self-organization. The hallmark of such a nonequilibrium state is the manifestation of critical exponents for salient features associated with the transient passage through a succession of metastable states, in our case, damping.[23] SOC has been successfully used to describe power-law scaling for electronic $1/f$ noise, earthquake frequency, river flow, brain activity, and economic activity.[23]

In the Appendix, we show that the strain fluctuation spectrum that is necessary to be consistent with the observed damping behavior is given by

$$\Delta \tilde{e}_{xx}(\omega) = \frac{2}{3} \left(\frac{C}{\omega} \right)^{\beta-1} \frac{M_S C}{\gamma E}, \tag{9}$$

where E is Young's modulus, β is from Eq. (4), and C is obtained by fitting the damping data of samples with Fe $<25\%$ in Fig. 7 to the functional form

$$\nu = C \lambda_s^{1/\beta}. \tag{10}$$

The fit yields $C=17\pm1$ MHz. However, we must note that the quality of the fit in Fig. 8 is not sufficient to dismiss the

0.1% possibility that ν and λ_s for samples with Fe$<25\%$ are correlated by chance.

We are now in a position to estimate the scale of the strain fluctuations that are necessary to observe the enhanced damping at low frequencies. At 1 GHz, the strain fluctuation amplitude $\Delta\tilde{e}_{xx}$ would need to be on the order of 7×10^{-7}. This is roughly one order of magnitude smaller than the largest magnetostriction values observed for the samples used in this study. It is therefore plausible that strain fluctuations may indeed be the reason for our observation of enhanced decay rates at low precession frequencies. The equivalent magnetostriction-dependent field fluctuations would be $H_s\Delta\tilde{e}_{xx}\approx414\lambda_s$ kA/m (5.2 λ_s kOe), where H_s is defined in the Appendix. For a sample with $\lambda_s=10^{-5}$, the field fluctuations would be 4.1 A/m (0.05 Oe), well within the range of plausibility.

While the enhanced low-frequency damping is sharply reduced if the magnetostriction is kept small, the data are not well described by the model summarized in Eq. (10) with $\beta=2.2$ as seen in Fig. 7. Several reasons may explain the apparent noise in the data for the samples with larger values of magnetostriction. The most significant may be the variation in the residual strain from sample to sample due to a number of uncontrolled deposition parameters, including a lack of temperature control for the substrates during sputter deposition, and the possibility of inducing strain during the current mounting procedure. Thus, it will be necessary to control sample strain to elucidate these effects in future studies.

VII. CONCLUSIONS

If we omit the data for samples with Fe$>25\%$, then we may draw some conclusions about the trends we observed and speculate about their meaning. Both the rotatable anisotropy and the anomalous increase of the low-frequency decay rate in Permalloy can be suppressed by growing films close to zero magnetostriction. While both of these effects have been previously observed,[2,16] this study shows that either effect can be significantly reduced by adjusting the sample magnetostriction. However, while the rotatable anisotropy was vanishingly small for the sample with the smallest magnetostriction, the enhancement in the low-frequency decay rate was still significant. For the sample with $\lambda_s=7\times10^{-8}$, the decay rate varied from 0.0073 at 3.7 GHz to 0.011 at 0.9 GHz, an increase of 37% over the measured range of frequencies. Therefore, the anomalous decay rate is unlikely to be purely the result of magnetostrictive effects.

Some have proposed that the often observed anomalous low-frequency increase in the decay rate is the result of coupling to a distribution of spin-wave modes when finite-width CPW center conductors are used.[24] We plot the predicted decay rate as a function of frequency along with the data in Fig. 4 using Eq. 17 of Ref. 24. The observed low-frequency enhancement is much larger than would be predicted by the spin-wave theory for the samples with nonzero magnetostriction. For the sample with very small magnetostriction, the increase in damping at low frequencies is within a factor of 2 of the spin-wave theory. Thus, our inability to eliminate the low-frequency increase in damping may be partly attributed to the generation of a distribution of spin-wave modes. However, these results indicate that it would not be prudent to assume that the damping at low frequencies is dominated by finite CPW center conductor width effects for arbitrary materials.

These results suggest that substantial errors may be incurred when extrapolating dynamic properties for magnetic materials intended for practical applications from measurements outside the operational bandwidth. For example, the high-frequency anisotropy of head materials in disk drive systems is often assumed to be identical to the low-frequency anisotropy, as determined by quasistatic magnetometry.[12] Alternatively, the presumed damping for magnetic films used in high-speed applications is often derived from the spectral linewidth in a high-frequency ferromagnetic resonance measurement.[25] The data presented here suggest that both assumptions are prone to significant error, especially if the material in question has non-negligible magnetostriction. For example, the sample with 73% Ni and $\lambda_s=7\times10^{-6}$ has a static anisotropy of 410 A/m, as determined in the linear regime where $\chi=M_s/H_k$, but the dynamic anisotropy, as measured with the PIMM, is 925 A/m, larger by more than a factor of 2 as a result of including the additional rotatable anisotropy that is manifested at microwave frequencies.

ACKNOWLEDGMENT

The authors wish to express sincere gratitude to Robert Stamps for many helpful discussions, including his original suggestion as to the importance of plastic strain in our experiments.

APPENDIX

We begin by assuming that the enhanced decay rate at low frequencies is the result of time-dependent field fluctuations. The time-dependent field fluctuations are the result of an avalanche-like relaxation of the strain. Thus, by assuming that the distribution of fluctuations in the effective field is proportional to the distribution of fluctuations in the strain, we can estimate the magnitude of the strain fluctuations associated with the observed frequency dependence of damping.

We start by transforming temporal correlations into the frequency domain. The amplitude of the effective field fluctuations due to strain is given by $\Delta\tilde{H}(\omega)$. The relationship between field fluctuations (i.e., field-swept linewidth) and temporal fluctuations leading to damping is given by[26]

$$\eta(\omega)=\left.\frac{\partial\omega}{\partial H}\right|_{\omega}\Delta\tilde{H}(\omega), \tag{A1}$$

where we make use of Onsager's regression hypothesis[27,28] to identify the decay rate with the correlation time scale for fluctuations about the mean. Converting from field-swept linewidth to normalized decay rate for a thin film,[26] we obtain

$$\frac{2}{\tau\omega_M} = \alpha + \left.\frac{\partial\omega}{\partial H}\right|_{\omega} \frac{\Delta\tilde{H}(\omega)}{(\omega_M + 2\gamma\mu_0 H)}$$

$$\approx \alpha + \left.\frac{\partial\omega}{\partial H}\right|_{\omega} \frac{\Delta\tilde{H}(\omega)}{\omega_M}, \quad H \ll M_S. \tag{A2}$$

From the form of the frequency dependence of damping in Eq. (4), we conclude that

$$\left(\frac{\nu}{\omega}\right)^{\beta} = \frac{\Delta\tilde{H}(\omega)}{\omega_M} \left.\frac{d\omega}{dH}\right|_{\omega}, \tag{A3}$$

where

$$\left.\frac{d\omega}{dH}\right|_{\omega} \cong \frac{1}{2}\gamma\mu_0\left(\frac{\omega_M}{\omega}\right). \tag{A4}$$

We assume a power-law distribution for field fluctuations in the frequency domain

$$\Delta\tilde{H}(\omega) = \left(\frac{\omega_0}{\omega}\right)^{\eta}\Delta H_0. \tag{A5}$$

Inserting Eq. (A5) into Eq. (A3) and equating powers of ω allow us to conclude that

$$\beta = 1 + \eta. \tag{A6}$$

The magnitude of the field fluctuations are related to temporal fluctuations in the strain by

$$\Delta H_0 \approx H_s \Delta e_{xx}, \tag{A7}$$

where

$$H_s \doteq \frac{3\lambda_s E}{2\mu_0 M_S} \tag{A8}$$

and E is the modulus of elasticity, typically equal to 200 GPa for most metals.[20] It follows that the spectrum of strain fluctuations should have a similar form, with

$$\Delta\tilde{e}_{xx}(\omega) = \left(\frac{\omega_0}{\omega}\right)^{\eta}\Delta e_{xx}. \tag{A9}$$

Insertion of Eqs. (A5) and (A7) into Eq. (A3) results in a power-law dependence of the relaxation scaling frequency ν upon magnetostriction:

$$\nu = C\lambda_s^{1/(1+\eta)}, \tag{A10}$$

where

$$C \doteq \left[\frac{3}{2}\frac{\gamma E \Delta e_{xx}\omega_0^{\eta}}{M_S}\right]^{1/(1+\eta)}. \tag{A11}$$

Fitting the data in Fig. 7 to Eq. (A10), we estimate that $C = 17 \pm 1$ MHz. Solving for the strain fluctuation Δe_{xx}, we obtain

$$\Delta e_{xx} = \frac{2}{3}\frac{M_S C^{1+\eta}}{\gamma E \omega_0^{\eta}}. \tag{A12}$$

Substituting (A11) into (A9), we arrive at

$$\Delta\tilde{e}_{xx}(\omega) = \frac{2}{3}\left(\frac{C}{\omega}\right)^{\eta}\frac{M_S C}{\gamma E}. \tag{A13}$$

[1] R. J. Prosen, J. O. Holmen, and B. E. Gran, J. Appl. Phys. **32**, 91S (1961).
[2] R. Lopusnik, J. P. Nibarger, T. J. Silva, and Z. Celinski, Appl. Phys. Lett. **83**, 96 (2003).
[3] J. P. Nibarger, R. L. Ewasko, M. L. Schneider, and T. J. Silva, J. Magn. Magn. Mater. **286**, 356 (2004).
[4] P. T. Squire, Meas. Sci. Technol. **5**, 67 (1994).
[5] E. Klokholm and J. A. Aboaf, J. Appl. Phys. **52**, 2474 (1981).
[6] R. H. Dee and D. D. King, J. Appl. Phys. **73**, 6232 (1993).
[7] R. M. Bozorth, *Ferromagnetism* (Wiley, New York, 1993).
[8] L. J. Swartzendruber, V. P. Itkin, and C. B. Alcock, in *ASM Metals Handbook*, 6th ed., edited by H. Baker (McGraw–Hill, New York, 1992).
[9] T. J. Silva, C. S. Lee, T. M. Crawford, and C. T. Rogers, J. Appl. Phys. **85**, 7849 (1999).
[10] O. Karlquist, Trans. R. Inst. Tech. Stockholm 86, 3 (1954).
[11] A. B. Kos, T. J. Silva, and P. Kabos, Rev. Sci. Instrum. **73**, 3563 (2002).
[12] C. Alexander, J. Rantschler, T. J. Silva, and P. Kabos, J. Appl. Phys. **87**, 6633 (2000).
[13] N. X. Sun, S. X. Wang, T. J. Silva, and A. B. Kos, IEEE Trans. Magn. **38**, 146 (2002).
[14] M. L. Schneider, A. B. Kos, and T. J. Silva, Appl. Phys. Lett. **85**, 254 (2004).
[15] J. P. Nibarger, R. Lopusnik, Z. Celinski, and T. J. Silva, Appl. Phys. Lett. **83**, 93 (2003).
[16] J. P. Nibarger, R. Lopusnik, and T. J. Silva, Appl. Phys. Lett. **82**, 2112 (2003).
[17] B. Heinrich, J. F. Cochran, and R. Hasegawa, J. Appl. Phys. **57**, 3690 (1985).
[18] W. v. d. Linden, M. Donath, and V. Dose, Phys. Rev. Lett. **71**, 899 (1993).
[19] R. Stamps (private communication).
[20] R. C. O'Handley, *Modern Magnetic Materials* (Wiley, New York, 2000), pp. 218–239.
[21] P. Bak, C. Tang, and K. Wiesenfeld, Phys. Rev. Lett. **59**, 381 (1987).
[22] C. Tang and P. Bak, Phys. Rev. Lett. **60**, 2347 (1988).
[23] M. Paczuski, S. Maslov, and P. Bak, Phys. Rev. E **53**, 414 (1996).
[24] G. Counil, J.-V. Kim, T. Devolder, C. Chappert, K. Shigeto, and Y. Otani, J. Appl. Phys. **95**, 5646 (2004).
[25] N. Smith, J. Appl. Phys. **90**, 5768 (2001).
[26] C. E. Patton, in *Magnetic Oxides*, edited by D. J. Craik (Wiley, London, 1975), pp. 575–645.
[27] L. Onsager, Phys. Rev. **37**, 405 (1931).
[28] D. Chandler, in *Introduction to Modern Statistical Mechanics* (Oxford University Press, New York, 1987), Chap. 8.